Fabrication and characterization of an L3 nanocavity designed by an iterative machine-learning method

AUTHOR(S):

Shibata, Takeshi; Asano, Takashi; Noda, Susumu

APL Photonics

Fabrication and characterization of an L3 nanocavity designed by an iterative machine-learning method

Cite as: APL Photonics **6**, 036113 (2021); https://doi.org/10.1063/5.0040793
Submitted: 16 December 2020 • Accepted: 05 March 2021 • Published Online: 28 March 2021

Takeshi Shibata, Takashi Asano and Susumu Noda

APL Photonics ARTICLE scitation.org/journal/app

Fabrication and characterization of an L3 nanocavity designed by an iterative machine-learning method

Cite as: APL Photon. 6, 036113 (2021); doi: 10.1063/5.0040793
Submitted: 16 December 2020 • Accepted: 5 March 2021 •
Published Online: 29 March 2021

Takeshi Shibata,[1,a)] Takashi Asano,[1,b)] and Susumu Noda[1,2]

AFFILIATIONS

[1] Department of Electronic Science and Engineering, Kyoto University, Kyoto 615-8510, Japan
[2] Photonics and Electronics Science and Engineering Center, Kyoto University, Kyoto 615-8510, Japan

[a)] shibata.takeshi@qoe.kuee.kyoto-u.ac.jp
[b)] **Author to whom correspondence should be addressed:** tasano@qoe.kuee.kyoto-u.ac.jp

ABSTRACT

Optical nanocavities formed by defects in a two-dimensional photonic crystal (PC) slab can simultaneously realize a very small modal volume and an ultrahigh quality factor (Q). Therefore, such nanocavities are expected to be useful for the enhancement of light–matter interaction and slowdown of light in devices. In the past, it was difficult to design a PC hole pattern that makes sufficient use of the high degree of structural freedom of this type of optical nanocavity, but very recently, an iterative optimization method based on machine learning was proposed that efficiently explores a wide parameter space. Here, we fabricate and characterize an L3 nanocavity that was designed by using this method and has a theoretical Q value of 29×10^6 and a modal volume of 0.7 cubic wavelength in the material. The highest unloaded Q value of the fabricated cavities is 4.3×10^6; this value significantly exceeds those reported previously for an L3 cavity, i.e., $\approx 2.1 \times 10^6$. The experimental result shows that the iterative optimization method based on machine learning is effective in improving cavity Q values.

I. INTRODUCTION

Optical nanocavities that are based on artificial defects in a two-dimensional (2D) photonic crystal (PC) slab have attracted much attention as device elements for light control. This is because they can realize high quality-factor (Q) values while maintaining a very small modal volume V. The experimental Q values were initially limited to values of less than one thousand but increased to more than ten million over time owing to advances in fabrication accuracy, material purity, and cavity design.[1–4] The ratio Q/V is a performance index that describes the strength of the light–mater interaction in the cavity material, as well as the product between the photon storage time and the capability of the cavity for dense integration.[5] Therefore, by increasing Q/V, a higher performance can be delivered in applications such as nanolasers,[6–9] bio-/chemical sensing devices,[8,9] bistable memories,[10] second-harmonic generation,[11] quantum information processing,[12,13] Si Raman lasers,[14] and dynamic control of photons.[15–18]

The Q value of a given PC nanocavity design [design Q value (Q_{design})], as well as V, depends on the cavity structure. It is known that the former, in particular, is not only determined by the cavity type; Q_{design} can be improved by several orders of magnitude by fine-tuning the positions of the air holes that define the cavity,[2–5,19–24] while V does not change so strongly except in cavity types based on electric-field concentration, such as those using slits,[25] and in cavity types based on the direct design of the confinement potential.[22–24] The Q value of a fabricated cavity [experimental Q value (Q_{exp})] is lower than Q_{design} due to factors such as the deviations of the actual structure from the designed structure or light absorption by the material.[26] However, since the achievable maximum of Q_{exp} of a cavity is restricted by its Q_{design}, the optimization of the cavity design (e.g., the hole pattern) is important. In Table I, we summarize some optimization results of Q_{design} values that have been obtained for different 2D PC cavity types, such as the L3 cavity,[2,27–30] the heterostructure cavity,[3,4,26] the H0 cavity,[27,31] the L4/3 cavity,[32] the locally width-modulated line-defect cavity (A1 cavity),[22,33] and the

TABLE I. Summary of the improvements in Q_{design} due to structural optimization and the resulting Q_{exp} values for various different cavity types. Here, Q values excluding the load of the excitation waveguides are used for comparison, except for Q_{exp} of the heterostructure cavities. The superscripts a, b, and c indicate the medians that were obtained by evaluating 21, 30, and 2 fabricated cavities, respectively. This table is for cavities fabricated from Si. The data of the cavity mode volume V (in units of λ^3/n^3) as well as the ratio Q_{exp}/V (in units of n^3/λ^3) are also provided.

Cavity type	Optimization method	Optimized degrees of freedom	Before optimization		After optimization				References
			V	Q_{design}	V	Q_{design}	Q_{exp}	Q_{exp}/V	
L3	Gaussian envelope	1	0.61	7×10^3	0.61	4.5×10^4	4.5×10^4	7.4×10^4	2
L3	Genetic algorithm	5	0.61	7×10^3	0.95	4.1×10^6	1.96×10^6 (1.1×10^{6a})	2.1×10^6 (1.2×10^{6a})	27 and 28
L3	Leaky mode visualization	9	0.61	7×10^3	0.75	4.2×10^6	2.1×10^6	2.8×10^6	29 and 30
Hetero-structure	Gaussian envelope	2	1.2	1×10^6	1.3	2×10^7	1×10^6	8×10^5	3 and 26
Hetero-structure	Leaky mode visualization	4	1.3	2×10^7	1.5	1.3×10^8	1.1×10^7 (6.9×10^{6b})	7.3×10^6 (4.6×10^{6b})	4 and 36
H0	Genetic algorithm	7	0.23	2.8×10^5	0.34	1.7×10^6	4.5×10^5	1.3×10^6	27 and 31
L4/3	Particle swarm	11	0.35	3.3×10^4	0.32	2.09×10^7	...	...	32
A1	Manual	1	1.4	5×10^6	1.7	7×10^7	1.3×10^6	7.6×10^5	22 and 33
Bi-chromatic	Manual	1	0.7	4×10^5	1.2	1.3×10^9	1.2×10^6	1×10^6	23 and 24
L3	Particle swarm	27	0.59	6.5×10^3	1.1	1.9×10^8	...	...	41
Hetero-structure	Machine learning	25	1.5	1.4×10^8	1.5	1.6×10^9	1.1×10^7 (7.8×10^{6b})	7.3×10^6 (5.2×10^{6b})	35 and 36
L3 (this work)	Machine learning	25	0.61	7×10^3	0.70	2.9×10^7	4.3×10^6 (3.7×10^{6c})	6.1×10^6 (5.3×10^{6c})	40, this work

effective bichromatic potential cavity,[23,24] together with the theoretical V values in units of (λ^3/n^3) (here, λ is the resonant wavelength of the cavity and n is the refractive index of the cavity material).[34] It can be confirmed that Q_{design} increases by optimizing the cavity structure parameters. Several different methods have so far been proposed for the optimization of the hole positions in the PC, e.g., the consideration of the envelope function of the electromagnetic field distribution,[2,3,21–24] the use of a genetic algorithm,[27,28,31] the visualization of the leaky-mode distribution,[4,29,30] particle swarm optimization,[32] and the use of machine learning.[35]

Due to the problems of the cost of manual tuning, and even computation time in the case of automatic tuning, the above-mentioned methods, except for machine learning, can usually only exploit a part of the high degree of freedom that is provided by the hole positions of a 2D PC cavity structure (while there are 20–30 degrees of freedom under symmetry constraints, the number of parameters that could be adjusted simultaneously was about 10 or smaller). To make sufficient use of the high degree of the structural freedom of a 2D PC nanocavity, machine learning can be used to generate a regression function (in the parameter space) that predicts Q_{design} based on the hole pattern that forms the cavity.[35] The regression function can then be used to calculate the gradient of the Q value with respect to the hole positions and updates the hole positions of a considered candidate pattern in such a way that the Q value increases.[35] By applying this method to the heterostructure cavity, we were able to improve Q_{design} from 140×10^6 [with $V = 1.5\ (\lambda^3/n^3)$] to 1600×10^6 [with $V = 1.5\ (\lambda^3/n^3)$],[35] and in the experiments, we succeeded in improving the Q_{exp} distribution.[36] After the publication of these results, attempts to optimize cavities with the help of machine learning have increased significantly.[37] Although even tuning of a few parameters can lead to a high Q_{design},[22–24] optimization techniques that enable tuning of a large number of structural parameters are important because such a tuning capability is inevitable for more versatile purposes, such as simultaneous improvement of different target parameters of a cavity.[32,38]

However, the number of tuning parameters is not the only important factor in optimization. For example, because the prediction in the above-mentioned machine-learning method becomes more incorrect as the new pattern departs from the vicinity of the parameter space region of the initial training dataset, it has not been possible to apply this method to optimizations where large shifts in the hole positions are required to find a significantly improved cavity (In the case of the above-mentioned results, the largest amount of shift was about 2%–3% of the lattice constant.). To solve this issue, a method has been proposed that additionally determines the Q_{design} values of the final candidate structures by a first-principles method, adds them to the training dataset, and then iterates these steps (i.e., generates a regression function, improves the candidates, evaluates their Q_{design} values by first-principles, and then adds these values to the training dataset).[39] The advantage of this iterative optimization method is the combination of a relatively high number of parameters and the automatic expansion of the training dataset

based on the experience of the neural network to reach the parameter space region of the more optimized structure. This can significantly reduce the size of the training dataset required to reach a given degree of optimization. By applying this method to optimize 25 cavity parameters of an L3 cavity with a low initial Q_{design} of seven thousand, we obtained a pattern with a Q_{design} of 29×10^6 and a small V of 0.7 (λ^3/n^3).[40] The maximum shift in the hole positions that was introduced in this case is 20% of the lattice constant. This Q_{design} is much larger than 4×10^6 obtained in the case of the optimization by the genetic algorithm and the leaky-mode visualization method.[27,30] However, an experimental verification with respect to this iterative optimization technique has not yet been performed.

Although there are cavity designs that exhibit even higher Q_{design} values, they usually also exhibit an increased V (see Table I). For example, while a work using particle swarm reported a much larger Q_{design} of 190×10^6, the obtained V was 1.1 (λ^3/n^3).[41] However, because the experimental Q factors are limited to values below 10×10^6 with the present fabrication technologies, it is important to realize cavity designs with $Q_{design} \gg 10 \times 10^6$ while maintaining a small V. An optimized L4/3 cavity with a Q_{design} of 21×10^6 and a V of 0.32 (λ^3/n^3) has been reported,[32] but this design has not yet been verified experimentally. Therefore, the experimental verification our L3 cavity design[40] optimized by the iterative optimization method is significant for further development of devices.

In this work, we fabricate samples with the L3 cavity structure designed by our iterative optimization method based on machine learning and verify the effectiveness of this optimization method experimentally. We obtain one cavity with an unloaded Q_{exp} of 4.3×10^6, and the median unloaded Q_{exp} of the cavities with the largest cavity–waveguide distance and hole radii within 102.5 ± 2 nm is 3.7×10^6. These values significantly exceed the corresponding values of the previously reported L3 cavities, i.e., about 2.1×10^6 and 1.1×10^6, respectively (see Table I).

II. CAVITY DESIGN AND THEORETICAL ANALYSIS

In Fig. 1(a), we show the designed cavity structure (air-hole pattern) of the L3 nanocavity investigated in this work. The basic PC structure consists of air holes located at the sites of a triangular lattice on the Si slab with a refractive index n of 3.46 and a slab thickness t of 220 nm. The hole radius is r = 102.5 nm (= 0.25 a) for all air holes, where a is the basic lattice constant of 410 nm.

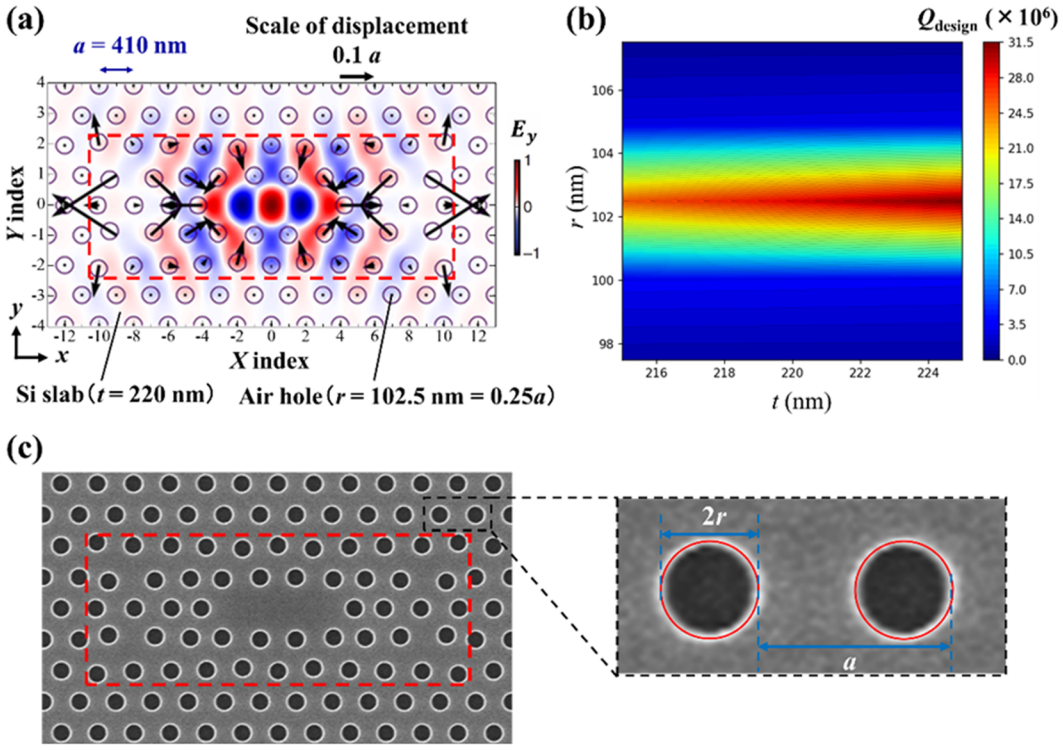

FIG. 1. The L3 cavity structure designed by the iterative optimization method based on machine learning. (a) The structure of the designed L3 cavity. The distribution of the electric field in the y-direction, E_y, is visualized using red and blue for positive and negative values, respectively. The red broken rectangle indicates the holes considered for the optimization. (b) The calculated result of the dependences of Q_{design} of the cavity in (a) on the average air-hole radius and the slab thickness. (c) Scanning electron microscopy (SEM) image of a fabricated L3 cavity. The area indicated by the red broken rectangle in Fig. 1(c) corresponds to that in Fig. 1(a). As shown in the magnified view indicated by the black broken rectangle, we estimated the hole radius from the ratio between the lattice constant and the diameter evaluated at the centerline of the broad white ring at the hole edge.

The L3 nanocavity is formed by removing three holes from this basic PC structure. In addition, the positions of the air holes within the red broken rectangle (extension: 21 columns × 5 rows) in the vicinity of the cavity have been adjusted according to the iterative optimization method based on machine learning.[40] In particular, for this optimization, we employed all three types of artificial losses described in Sec. 3.3 of Ref. 39. In Fig. 1(a), the black arrows indicate the changes in the hole positions with respect to the hole positions before optimization. A discussion of the characteristics of this cavity structure is given in Appendix A. For the present fabrication procedure, we discretized the air-hole shifts at the resolution of the electron beam lithography (EBL) system (0.125 nm). The details of the hole position shifts after discretization are shown in Table II. Moreover, we also confirmed Q_{design} of the cavity with the discretized hole positions by three-dimensional finite-difference time-domain (FDTD) analysis. There was almost no difference compared to the Q value before discretization, and we obtained $Q_{design} = 29 \times 10^6$ and $V = 0.70\ (\lambda^3/n^3)$.

Prior to fabrication, we also examined the impact of the expected imperfections of the real device on the Q value. Three types of losses are considered: fabrication errors in the hole pattern, absorption by the material, and coupling to the excitation waveguide.

First, to fabricate such a nanostructure pattern, an EBL process and a transfer of the pattern by dry-etching are used. Here, small fluctuations in the fabricated hole shape are unavoidable. With respect to PC nanocavities, it is known that the influences of these fluctuations can be characterized by converting them to fluctuations in the air-hole radius and position.[26,42,43] In our presently used fabrication conditions, the empirical standard deviation of these parameters is less than 0.5 nm.[4,36,43] To determine the resulting loss, $1/Q_{scat}$, we generated 100 random air-hole patterns based on the structure shown in Fig. 1(a) and calculated their cavity Q values. The random patterns included fluctuations in the hole radius and position with a standard deviation of 0.41 nm (one thousandth of the lattice constant a), and the resulting loss $1/Q_{scat} = 1/(7.7 \times 10^6)$ was obtained by subtracting the inverse of the above-mentioned Q_{design} of the ideal structure from the average of the inverse of the Q values of these random structures. Note that this value is almost the same as the loss of $1/(7.9 \times 10^6)$ that was obtained for a heterostructure cavity when we used the same standard deviation for the calculation of $1/Q_{scat}$.[4,44] Thus, we confirmed that the present optimized L3 cavity is not particularly weak with respect to structural imperfections. The explanation for this result is provided in Appendix B.

We also examined the impact of the average deviation of the air-hole radius from the optimum radius. This is necessary because the average value can change by a few nanometers.[30] The reason for this is that the overall hole radius depends on the etching conditions. On the other hand, the average deviation of the hole position defined by the electron beam is, in principle, sufficiently small because the EBL accuracy is sufficiently stable owing to the laser interferometer stage in the EBL system. We also examined the effect of the thickness variation of the top Si slab of the silicon-on-insulator (SOI) substrate used in the fabrication because the slab thickness varies by about 1–2 nm depending on the position in the wafer. The result in Fig. 1(b) evidences that Q_{design} of the presently considered cavity has a small dependence on the slab thickness, but Q_{design} decreases to one third if the hole radius deviates by ±2 nm from the optimum value. Such a behavior has been also reported for an L3 cavity that has been optimized by the visualization of the leaky modes.[30] The reason for this behavior is discussed in Appendix B. Here, it should be mentioned that, even if the average air-hole radius is deviated by about ±2 nm, Q_{design} would still be about two times larger than Q_{design} of the L3 cavities that have been optimized by conventional methods and have optimum hole radii.[27,30]

Second, it is known that a fabricated cavity has an additional loss that is caused by light absorption due to both the material and imperfections of its surface.[4,45] The magnitude of this loss, $1/Q_{abs}$, can be changed by applying surface treatments, but from our past experience it is expected that it is at least on the order of $1/(12 \times 10^6)$.[4] By considering the additional losses ($1/Q_{scat}$ and $1/Q_{abs}$), the theoretical Q value ($:Q_{theory}$) becomes about 4×10^6 in the case of the optimum average hole radius, and in the case that the average hole radius deviates by ±2 nm, it is expected that $Q_{thoeory}$ becomes about 3.2×10^6.

Third, in order to actually measure the value of Q_{exp}, it is necessary to add a waveguide for excitation in the vicinity of the cavity. A design with an appropriate coupling strength (several times larger than the Q value of the cavity alone) is required because a reduction in Q_{exp} occurs due to the coupling to the waveguide.[46] We decided to use a width of $1.1 \times \sqrt{3}a$ for the excitation waveguide. To clarify the impact of the waveguide, we changed the distance between the cavity and the waveguide, d, from 7 to 9 rows, and determined the changes in the Q values. The waveguide-coupling losses, $1/Q_{wg}$, for d = 7, 8, and 9 rows determined by three-dimensional FDTD analysis were $1/(0.84 \times 10^6)$, $1/(4.9 \times 10^6)$, and $1/(12 \times 10^6)$, respectively. Hereafter, we denote Q_{exp} including the waveguide-coupling loss $1/Q_{wg}$ as the loaded Q_{exp} or Q_{exp}^{loaded}, and Q_{exp} excluding $1/Q_{wg}$ as the unloaded Q_{exp}.

TABLE II. The x- and y-shifts of each hole in the L3 cavity structure in the red broken rectangle shown in Fig. 1(a). These shift amounts are discretized at the resolution of 0.125 nm of the EBL system. Because the shifts were introduced in a manner such that the mirror symmetries with respect to the x- and y-axis are retained, only data from the first quadrant are provided. The holes located on the x- or y-axis have only one degree of freedom, while the other holes have two degrees of freedom, resulting in 25 degrees of freedom in total.

X index	Y index	X shift (nm)	Y shift (nm)
4	0	52.000	0.000
6	0	−21.000	0.000
8	0	−10.375	0.000
10	0	19.000	0.000
1	1	−2.875	−2.250
3	1	19.250	−22.750
5	1	−29.875	−18.750
7	1	−37.625	−34.375
9	1	77.500	−49.250
0	2	0.000	6.000
2	2	−8.375	−28.875
4	2	−6.250	−7.750
6	2	−14.875	4.000
8	2	4.000	7.500
10	2	6.625	39.500

III. FABRICATION AND OPTICAL CHARACTERIZATION

Regarding the fabrication of the nanocavities, here we used a SOI substrate, and after the formation of the PC pattern in the top Si layer, we fabricated an air-bridge structure by removing the buried oxide (BOX) layer by hydrofluoric acid (HF). The average thicknesses of the top Si layer and the BOX layer of the SOI substrate were 220 and 3000 nm, respectively. For the formation of the PC pattern, we employed EBL and inductively coupled plasma etching with SF_6-based gas. As mentioned above, the resolution of the EBL system was 0.125 nm. Even if all electron-beam-written radii are exactly equal, the radii of the formed holes change depending on the etching conditions. To experimentally verify the relation between Q_{exp} and the average air-hole radius, we fabricated several cavities with different average hole radii by slightly changing the hole radius used in each EBL process. We fabricated nine types of cavities: Their average air-hole radii after the etching process were in the range from 99 to 113 nm in equally spaced intervals. For each of the nine sample types, we fabricated one long and thin PC pattern (total length 2.4 mm) and placed a long waveguide for the excitation at the center of the PC pattern. In the vicinity of the waveguide, the cavities were placed with a sufficient distance between them in the direction of the waveguide. In this way, we placed several cavities with different values of d along a single excitation waveguide. For each cavity-parameter set, two cavities were prepared.

A SEM image of one of the fabricated cavities is shown in Fig. 1(c). The fabricated structure well reflects the designed hole pattern. The air-hole radii can be evaluated from such SEM images by assessing the ratio of the air-hole radius (measured from the center of the air hole to the white ring at the hole edge) to the lattice constant and multiplying the result by the known lattice constant of the PC design. The lattice constant was measured in a location that contains no intentional shift in the hole positions. Note that the white ring at the hole edge has a certain linewidth, and we evaluated the hole radius by measuring the distance from the center of the hole to the centerline of the broad ring. The threshold used to identify the white ring is approximately set to the highest brightness observed at the flat region of the slab. The accuracy of the evaluated value is about one fifth of the width of the white ring and is about ±2 nm in our case. Moreover, to avoid a possible pollution of the sample surface due to the SEM characterization, the characterization of the hole radii was performed on a simultaneously fabricated reference sample. Here, we characterized the two hole radii of the structures with the largest and smallest holes and estimated the radii in between by using a linear approximation.

For the optical characterization of the fabricated cavities, we first measured the resonance wavelength λ_0 by using a wavelength-tunable laser. Then, we determined the photon lifetime in the cavity, τ, from a time-resolved measurement and calculated Q_{exp}^{loaded} using the relation $Q_{exp}^{loaded} = \frac{2\pi c}{\lambda_0}\tau$ (here, c is the speed of light in vacuum).[47] We used the time-correlated single photon counting (TCPSC) method to measure the decay of the light emitted from the cavity after resonant excitation using an optical pulse with a width of 10 ns. In Fig. 2(a), we show the correlation between Q_{exp}^{loaded} and the average air-hole radius (note that the cavities with r = 101.2 nm and 109.7 nm were not measured). The colors of the data points are used to clarify the dependence on the distance d between the cavity and the waveguide. The purple, green, and orange dots are the data for d = 7, 8, and 9 rows, respectively. (The number of data points for d = 7, 8, and 9 rows is not equal because not all fabricated cavities were characterized optically.) From Fig. 2(a), we find that Q_{exp}^{loaded} exhibits a distribution with a peak at a hole radius of about 104.6 nm. Moreover, the larger the value of d is, the higher Q_{exp}^{loaded} becomes. The highest Q_{exp}^{loaded} among these cavities is 2.7×10^6 obtained for the cavity with d = 9. The broken curves in Fig. 2(a) are theoretical predictions (Q_{theory}^{loaded}) that consider the scattering loss ($1/Q_{scat}$) due to the fluctuations in the hole radius and hole position, the absorption loss ($1/Q_{abs}$), the loss due to the coupling to the waveguide ($1/Q_{wg}$),

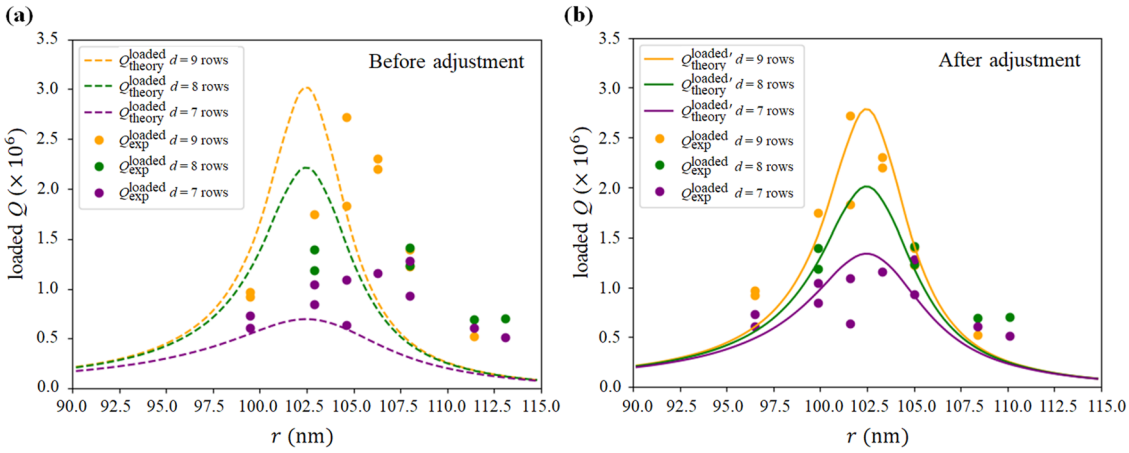

FIG. 2. The relation between the experimental loaded Q value and the average air-hole radius r, and its dependence on the cavity–waveguide distance d. (a) Relation when r is evaluated as the distance from the center of the air hole to the centerline of the white ring in the SEM image. The purple, green, and orange broken curves are the corresponding theoretically predicted values for $1/Q_{wg} = 1/(0.84 \times 10^6)$, $1/(4.9 \times 10^6)$, $1/(12 \times 10^6)$. (b) Relation when the evaluated r is reduced by 15% of the width of the white ring in the SEM image. The colored solid curves are the theoretical predictions when the losses due to coupling to the waveguide are changed to $1/(2 \times 10^6)$, $1/(4 \times 10^6)$, and $1/(9 \times 10^6)$.

and the influence of the deviation of the average hole radius from the optimum value, as explained above. By comparing the experimental and the theoretically predicted values, it is found that the experimental values are overall shifted toward larger hole radii by about 3 nm and that the dependence on d is slightly weaker. To explain the shift by about 3 nm, we can consider the measurement error in the hole-radius assessment by SEM (about ±2 nm) and the deviation between the structures of the sample used for the hole-radius assessment and that actually used in the optical measurements. Note that the theory and experiment agreed when the hole-radius evaluation criterion in the SEM images was changed to the distance from the center of the hole to a position closer to the inner edge of the white ring by 15% of the width of the white ring. The relation between the $Q_{\mathrm{exp}}^{loaded}$ value and the hole radius evaluated with this corrected criterion is shown in Fig. 2(b). Regarding the dependence on d, a good agreement with the experimental results was obtained when we assumed $1/Q_{\mathrm{wg}} = 1/(2 \times 10^6)$, $1/(4 \times 10^6)$, and $1/(9 \times 10^6)$ for d = 7, 8, and 9 rows, respectively [$Q_{\mathrm{theory}}^{loaded\prime}$; the purple, green, and orange solid curves in Fig. 2(b)]. The $1/Q_{\mathrm{wg}}$ values derived in the above-mentioned FDTD calculation are $1/(0.84 \times 10^6)$, $1/(4.9 \times 10^6)$, $1/(12 \times 10^6)$, respectively, but we believe that this degree of difference is reasonable. When we analyze the overall distribution of the experimental results for d = 9 rows in Fig. 2(b), we find that an $Q_{\mathrm{exp}}^{loaded}$ of about 2×10^6 can be obtained even if the hole radius deviates from the optimum value by ±2 nm.

As the intervals between the nine different average radii of the samples fabricated in this work were about 1.6 nm, there is the possibility that the experimental optimum radius is not among the fabricated average radii. To find the optimum radius experimentally, we tried to adjust the hole diameter by using a post-process. Note that the interval of 1.6 nm is not the accuracy limit of the EBL system, and thus, a post-process is not necessary if it is more feasible to prepare additional samples with different design hole radii. For the adjustment, we used a method that consists of forming a thin oxide layer on the sample surface by high-temperature oxidation and subsequently removing the surface oxide layer using diluted hydrofluoric acid (DHF). While the degree of diameter-change depends on the details of the oxidation conditions, it has been reported that about less than 1 nm of material is removed from the Si surface during each cycle of this process.[4] In this process, the size of the hole increases, and at the same time, the slab thickness decreases. However, as shown in Fig. 1(b), the impact of the slab-thickness decrease on the Q value is small. We can accurately determine the amount of the removed Si, i.e., the change in the average air-hole radii, from the change in the cavity resonance wavelength due to the post-process. With the conditions used in this work, λ_0 was reduced by 3.3–3.4 nm during each cycle of the post-process. By estimating the amount of removed material that corresponds to this shift toward shorter wavelengths using FDTD calculations, we found that this decrease in λ_0 is equivalent to uniform removal of 0.7 nm of the material (Si) from all surfaces of the sample, that is, the top and bottom surfaces of the slab and at the hole walls. Based on this result, we determined the average hole radii after the post-process by adding 0.7 nm for each post-process cycle to the hole radii that was determined from the SEM image by using the criterion defined for Fig. 2(b).

The relations between the $Q_{\mathrm{exp}}^{loaded}$ value and the hole radius before post-processing, after one post-process cycle, and after two post-process cycles for the samples with d = 9 rows are shown in Fig. 3 by the orange, blue, and red data points, respectively. Moreover, to make the changes clearer, each change in the $Q_{\mathrm{exp}}^{loaded}$ value of a cavity due to a post-process cycle is indicated by a green arrow (note that not all samples have been measured at each processing step). From Fig. 3, it is found that the $Q_{\mathrm{exp}}^{loaded}$ values of the cavities that had an initial hole radius smaller than 102.5 nm increase due to the post-processing and the $Q_{\mathrm{exp}}^{loaded}$ values of the cavities that had larger radii decrease. This trend agrees well with the theoretical prediction (orange solid curve). Moreover, $Q_{\mathrm{exp}}^{loaded}$ of the cavity with the highest initial $Q_{\mathrm{exp}}^{loaded}$ among our samples (2.7×10^6) increased further due to the post-processing. With this, we confirmed that this cavity had a structure with an average hole radius slightly (about 0.7 nm) below the optimum hole radius. The lifetime measurement result of this cavity after one post-process cycle is shown in Fig. 4. From Fig. 4, a photon lifetime of 2.36 ns is obtained, which corresponds to a $Q_{\mathrm{exp}}^{loaded}$ of 2.9×10^6. The unloaded Q_{exp} of this cavity is 4.3×10^6, which is obtained by subtracting the waveguide coupling loss evaluated in Fig. 2(b) [$1/Q_{\mathrm{wg}} = 1/(9 \times 10^6)$].

The median $Q_{\mathrm{exp}}^{loaded}$ of the fabricated cavities with d = 9 rows and appropriate hole radii (within 102.5 ± 2 nm) is 2.25×10^6 before post-processing and 2.6×10^6 after the second post-process cycle. The corresponding median unloaded Q_{exp} values are 3.0 and 3.7×10^6, respectively. When we define the yield as the ratio of the number of cavities with $Q_{\mathrm{exp}}^{loaded} > 2 \times 10^6$ to the number of cavities with average hole radii within 102.5 ± 2 nm, the yield was 75% before post-processing and 100% after the first and second post-process cycles. These values demonstrate the robustness of this L3 cavity to fabrication-dependent fluctuations.

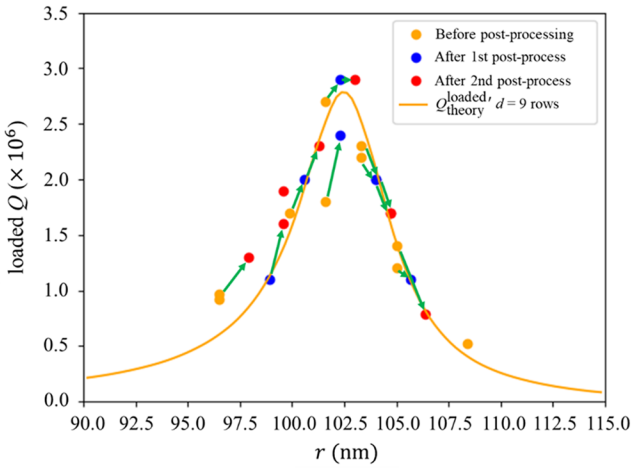

FIG. 3. The relations between $Q_{\mathrm{exp}}^{loaded}$ and the hole radius measured before post-processing (orange points), after one post-process cycle (blue points), and after two post-process cycles (red points) for the samples with d = 9 rows. The hole radii shown are those determined using the criterion defined for Fig. 2(b). Each green arrow indicates a change in the Q value of a single cavity due to one or two post-process cycle(s). The orange solid curve is the theoretical prediction [the same curve as in Fig. 2(b)].

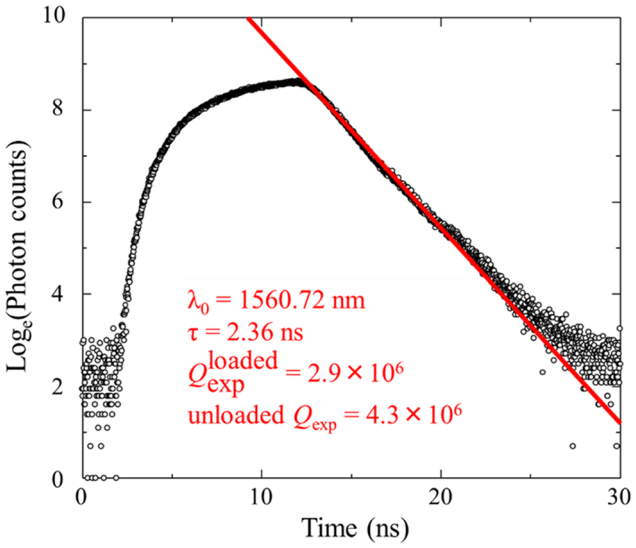

FIG. 4. The result of the time-resolved measurement of the emission from the cavity with the longest photon lifetime among the post-processed samples. The resonance wavelength is 1560.72 nm, and the photon lifetime is 2.36 ns, which corresponds to a Q_{exp}^{loaded} of 2.9 × 10^6 and an unloaded Q_{exp} of 4.3 × 10^6.

IV. DISCUSSION

Figure 4 shows that it was possible to fabricate an L3 cavity with an unloaded Q_{exp} of 4.3 × 10^6. This value significantly exceeds the previously reported top experimental L3-cavity unloaded Q values of 1.96 × 10^6 (the directly measured Q value of the cavity alone)[28] and 2.1 × 10^6 (the Q value of the cavity alone obtained by removing the loss due to the coupling to the waveguide from Q_{exp}^{loaded}).[30] Additionally, the modal volume of our cavity design, V = 0.70 (λ^3/n^3), is smaller than those of the cavity designs used in these two previous investigations, i.e., V = 0.96 (λ^3/n^3)[28] and 0.75 (λ^3/n^3).[29] In our present work, the median unloaded Q_{exp} after the second post-process cycle was 3.7 × 10^6 (obtained by evaluating two cavities), which significantly exceeds the median value that has been reported for an L3 cavity optimized by a genetic algorithm (1.1 × 10^6, obtained by evaluating 21 cavities).[28] It is plausible that a large part of this improvement is due to an increase in Q_{design} from 4 × 10^6 (previous designs)[28,30] to 29 × 10^6 (the present design). This explanation is supported by the fact that the predicted unloaded Q_{exp} would become 2.2 × 10^6 (which is similar to the values in Ref. 28) if Q_{design} of the present structure decreased to 4 × 10^6. This result indicates that the recently proposed iterative optimization based on machine learning can result in a clear positive effect even in the presence of imperfections such as fabrication-induced fluctuations in the hole radius and hole position.

For comparison with values of other investigations, it should be mentioned that the loss due to the coupling to the waveguide, $1/Q_{wg}$, is usually evaluated experimentally from the waveguide transmission spectrum.[46] However, because it was difficult to measure a reliable transmission spectrum in the presently employed structure, wherein many cavities are coupled to the single, long (2.4 mm) waveguide, we were not able to estimate this coupling loss experimentally. Instead, we evaluated $1/Q_{wg}$ by fitting the Q_{exp}^{loaded} values for samples with different waveguide–cavity distances d. As explained in Sec. III, the obtained value of Q_{wg} for d = 9 rows was comparable to the value obtained from the 3D-FDTD simulation without structural fluctuation (9 × 10^6 and 12 × 10^6, respectively). For the estimation of the degree of the uncertainty in Q_{wg} in the presence of structural fluctuations, we performed one hundred 3D-FDTD simulations of the cavity pattern for d = 9 rows including random fluctuations in the hole radius and position with a standard deviation of 0.41 nm. We obtained an average Q_{wg} value of 9.9 × 10^6, and the corresponding standard deviation was 1.1 ×10^6. When we consider a Q_{wg} of 9.9 × 10^6 ± 1.1 × 10^6, the unloaded Q_{exp} of the cavity with Q_{exp}^{loaded} = 2.9 × 10^6 (Fig. 4) lies in the range of 3.9–4.3 × 10^6. When we assume that the predicted standard deviation of 1.1 × 10^6 applies to the experimentally fitted Q_{wg} of 9 × 10^6, the estimated range of the unloaded Q_{exp} value is 4.1–4.6 × 10^6. Therefore, we consider that the unloaded Q_{exp} of the cavity with Q_{exp}^{loaded} = 2.9 × 10^6 lies within a range of 3.9–4.6 × 10^6.

An additional aspect of the fabrication is that we fabricated nine types of cavities with different average hole radii in order to confirm the results of the theoretical prediction. A result that is worth noting is that the dependence of the Q_{exp} on the hole radius almost coincides with the theoretical prediction if the air-hole radius is appropriately estimated from the SEM image. Therefore, it is considered that by adding a few cavities with different average hole radii as a set of cavities for adjustment on one chip in addition to the main cavity-set, the necessity of an adjustment of the hole radius of the main cavity-set can be judged from the measurement of the Q values of the cavity set for adjustment.

V. CONCLUSION

We have reported on the fabrication and performance characterization of an L3 cavity with a design Q value of 29 × 10^6. The design was obtained in a previous study by optimizing 25 degrees of freedom of the L3 cavity using an iterative optimization method based on machine learning. In this work, we obtained experimental results that well reflect the theoretical relationship between the Q value and the average hole radius, and thus, we have confirmed that a cavity with a complex hole pattern design can be actually fabricated. The ratio of cavities with an unloaded Q_{exp} > 2.6 × 10^6 (Q_{exp}^{loaded} > 2 × 10^6) to the cavities with d = 9 rows and appropriate average hole radii (within 102.5 ± 2 nm) was 75% before post-processing and 100% after the first and second post-process cycles. The obtained maximum unloaded and loaded experimental Q values were 4.3 × 10^6 (3.9–4.6 × 10^6 when considering the uncertainty in the waveguide coupling loss) and 2.9 × 10^6, respectively. These values largely exceed the previously reported unloaded experimental Q value of 2.1 × 10^6. Moreover, the obtained median unloaded and loaded experimental Q values were 3.7 and 2.6 × 10^6, respectively, both being significantly larger than the median unloaded experimental Q value of 1.1 × 10^6 reported previously. We consider that a large portion of this improvement can be attributed to an increase in the design Q value from 4 × 10^6 of the previous design to 29 × 10^6 of the present design. Our experimental results have shown that the iterative optimization method based on machine learning is effective

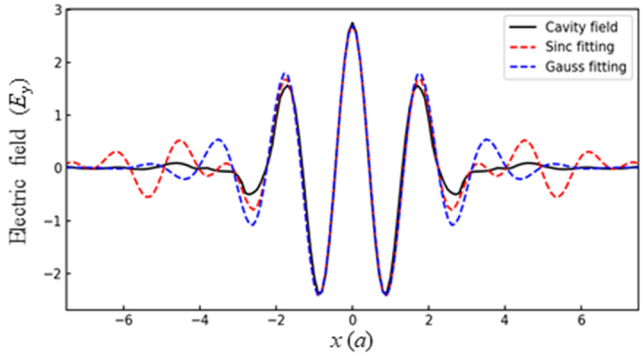

FIG. 5. Line plot (in the plane $y = 0$) of the E_y electric field distribution of the optimized L3 cavity shown in Fig. 1(a) (black solid curve). The result of the fits of the field to a sinc envelope function and a cosine function [$A\mathrm{sinc}(Bx)\cos(Cx)$, red dashed curve] and to a Gaussian envelope function and a cosine function [$A\exp(-x^2/B^2)\cos(Cx)$, blue dashed curve].

for the improvement of cavity Q values. We believe that exploiting the high degree of freedom in the design of 2D-PC nanocavities by machine learning will play an important role in optimization of not only single Q factor values but also other parameters of nanocavities.

ACKNOWLEDGMENTS

This work was partially supported by KAKENHI Grant No. 19H02629 and received funding from the New Energy and Industrial Technology Development Organization (NEDO) under Grant No. JPNP13004.

APPENDIX A: AIR-HOLE PATTERN AND ELECTRIC FIELD OF THE OPTIMIZED CAVITY

With respect to our present optimized cavity design, we noticed that many air holes tend to shift toward the center of the cavity along the direction normal to the contour of the electric field, although exceptions exist, as shown in Fig. 1(a). It is also interesting that the cavity-field envelope function in the plane of the x axis ($y = 0$) is more similar to a sinc function than to a Gaussian function, as shown in Fig. 5. Because the Fourier transform of a sinc function is a rectangular function while that of a Gaussian function is another Gaussian function, a sinc envelope function (in real space) is theoretically more appropriate to reduce leaky components.[20] These results indicate that our iterative machine learning method automatically detected a cavity design that had a mode field better than the Gaussian confinement.

APPENDIX B: RELATION BETWEEN LOSS AND AVERAGE HOLE RADIUS

First, we consider the reason why the scattering loss of the present optimized L3 cavity is comparable to that of the heterostructure in Ref. 4. It is known that the magnitude of the scattering loss is determined by $(\Delta P)^2 = (\epsilon \Delta V \times E)^2$,[48] where ΔV is the change in the dielectric volume due to a fluctuation, ϵ is the dielectric constant, and E is the electric field in that volume. Therefore, in the case that the magnitude of the fluctuation is independent of the hole size, the scattering loss due to small fluctuations in the air-hole radius and position is determined by the optical energy that is distributed at the edges of the air holes. The distribution of the optical energy at the air-hole edge in an L3 nanocavity is considered to be slightly larger than that in a heterostructure nanocavity because of the existence of air holes in the center row of the L3 cavity [e.g., see Figs. 1(a) and 6(a)]. However, the air-hole radius of the optimized L3 cavity used in this work (102.5 nm) is smaller than that of the heterostructure cavity used for comparison (110 nm), which partly compensates (by about 13%) the effect of the field distribution. As a result, the scattering loss of an optimized L3 cavity with $r = 102.5$ nm can be comparable to that of a heterostructure nanocavity with $r = 110$ nm. Although a difference between the tolerances to structural fluctuations of partially optimized L3 and heterostructure cavities has been reported,[49] it should be noted the structures investigated in this previous work are different from ours.

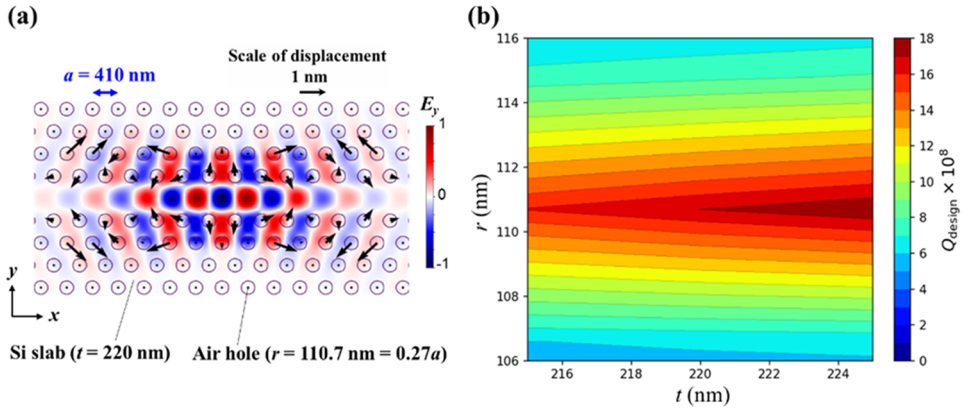

FIG. 6. The dependences of a heterostructure cavity designed by machine learning [Fig. 8(c) in Ref. 30] on structural parameters. (a) The structure of the optimized heterostructure cavity. The distribution of the electric field in the y-direction, E_y, is visualized using red and blue for positive and negative values, respectively. (b) The calculated result of the dependences of Q_{design} of the cavity in (a) on the average air-hole radius and the slab thickness.

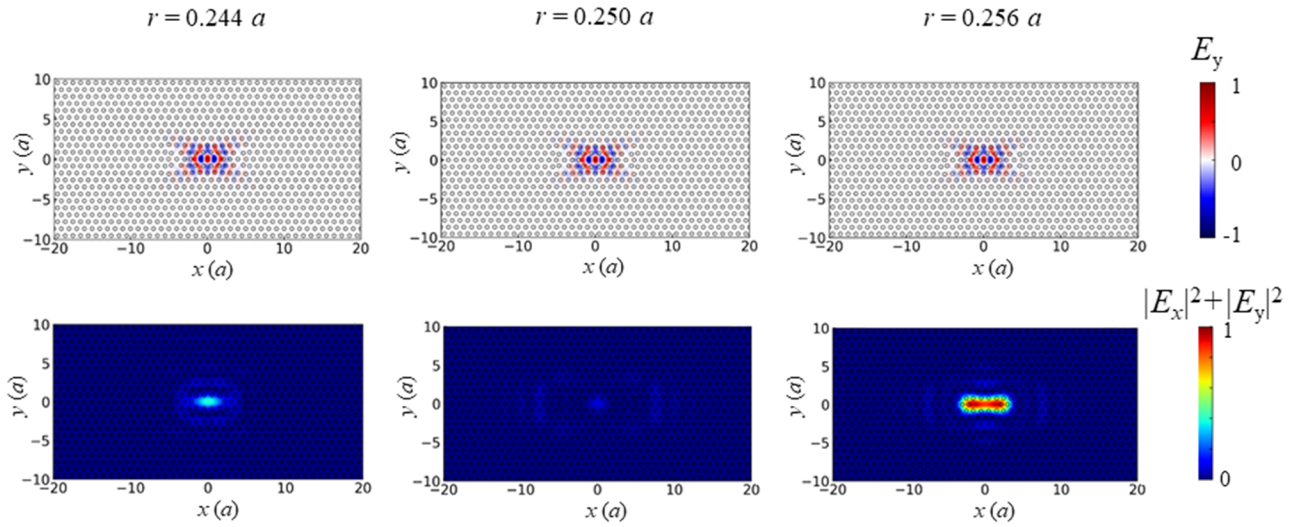

FIG. 7. Electric field distributions (top panels) and leaky component distributions (lower panels) of the optimized L3 cavity hole pattern for three different air-hole radii.

Second, we found that the dependence of Q_{design} on the average hole radius is weaker for the optimized heterostructure cavity, as shown in Fig. 6(b). This different tendency for different cavity types is attributed to a difference in the intensity of the radiation field that occurs if the air-hole positions are not tuned in accordance with the hole size. In other words, we consider that the hole shifts introduced during the optimization process lead to a subtle cancellation of the radiation field, and this cancellation can be destroyed by a change in the air-hole radius. Figure 7 shows the electric field distributions and the leaky component distributions[29] of three L3 cavities with the same optimized hole position pattern (optimized for $r = 0.25a$), but with three different air-hole radii. We can confirm that the electric field distributions are almost the same (Fig. 7, upper panels), while the intensities of the leaky components are very different (Fig. 7, lower panels). This result supports the explanation that a finely established far-field cancellation can be easily disturbed by a change in the air-hole radius. In such a situation, the radiation intensity can reach levels equivalent to the case without tuning. Such a degradation in Q_{design} can be considered more severe for cavities with a larger ratio between the initial and optimized Q_{design} values. The Q_{design} values of the present L3 nanocavity before and after our optimization are seven thousand and 29×10^6,[40] respectively, which differ by four orders of magnitude. On the other hand, the Q_{design} values before and after our optimization of the heterostructure nanocavity are 20×10^6 and 1600×10^6,[35,36] respectively, which differ by only two orders of magnitude. Therefore, the degradation of the Q factor is more severe for L3 cavities.

DATA AVAILABILITY

The data that support the findings of this study are available from the corresponding author upon reasonable request.

REFERENCES

[1] S. Noda, A. Chutinan, and M. Imada, "Trapping and emission of photons by a single defect in a photonic bandgap structure," Nature **407**, 608–610 (2000).
[2] Y. Akahane, T. Asano, B.-S. Song, and S. Noda, "High-Q photonic nanocavity in a two-dimensional photonic crystal," Nature **425**, 944–947 (2003).
[3] B.-S. Song, S. Noda, T. Asano, and Y. Akahane, "Ultra-high-Q photonic double-heterostructure nanocavity," Nat. Mater. **4**, 207–210 (2005).
[4] T. Asano, Y. Ochi, Y. Takahashi, K. Kishimoto, and S. Noda, "Photonic crystal nanocavity with a Q factor exceeding eleven million," Opt. Express **25**, 1769–1777 (2017).
[5] T. Asano and S. Noda, "Photonic crystal devices in silicon photonics," Proc. IEEE **106**, 2183–2195 (2018).
[6] S. Strauf, K. Hennessy, M. T. Rasher, Y.-S. Choi, A. Badolato, L. C. Andreani, E. L. Hu, P. M. Petroff, and D. Bouwmeester, "Self-tuned quantum dot gain in photonic crystal lasers," Phys. Rev. Lett. **96**, 127404 (2006).
[7] S. Matsuo, A. Shinya, T. Kakitsuka, K. Nozaki, T. Segawa, T. Sato, Y. Kawaguchi, and M. Notomi, "High-speed ultracompact buried heterostructure photonic-crystal laser with 13 fJ of energy consumed per bit transmitted," Nat. Photonics **4**, 648–654 (2010).
[8] M. Lončar, A. Scherer, and Y. Qiu, "Photonic crystal laser sources for chemical detection," Appl. Phys. Lett. **82**, 4648–4650 (2003).
[9] S. Kita, K. Nozaki, and T. Baba, "Refractive index sensing utilizing a cw photonic crystal nanolaser and its array configuration," Opt. Express **16**, 8174–8180 (2008).
[10] K. Nozaki, A. Shinya, S. Matsuo, Y. Suzaki, T. Segawa, T. Sato, Y. Kawaguchi, R. Takahashi, and M. Notomi, "Ultralow-power all-optical RAM based on nanocavities," Nat. Photonics **6**, 248–252 (2012).
[11] B.-S. Song, T. Asano, S. Jeon, H. Kim, C. Chen, D. D. Kang, and S. Noda, "Ultrahigh-Q photonic crystal nanocavities based on 4H silicon carbide," Optica **6**, 991–995 (2019).
[12] T. Yoshie, A. Scherer, J. Hendrickson, G. Khitrova, H. M. Gibbs, G. Rupper, C. Ell, O. B. Shchekin, and D. G. Deppe, "Vacuum Rabi splitting with a single quantum dot in a photonic crystal nanocavity," Nature **432**, 200–203 (2004).
[13] A. Faraon, A. Majumdar, D. Englund, E. Kim, M. Bajcsy, and J. Vučković, "Integrated quantum optical networks based on quantum dots and photonic crystals," New J. Phys. **13**, 055025 (2011).
[14] Y. Takahashi, Y. Inui, M. Chihara, T. Asano, R. Terawaki, and S. Noda, "A micrometre-scale Raman silicon laser with a microwatt threshold," Nature **498**, 470–474 (2013).

[15]Y. Tanaka, J. Upham, T. Nagashima, T. Sugiya, T. Asano, and S. Noda, "Dynamic control of the Q factor in a photonic crystal nanocavity," Nat. Mater. **6**, 862–865 (2007).
[16]Y. Sato, Y. Tanaka, J. Upham, Y. Takahashi, T. Asano, and S. Noda, "Strong coupling between distant photonic nanocavities and its dynamic control," Nat. Photonics **6**, 56–61 (2011).
[17]R. Konoike, H. Nakagawa, M. Nakadai, T. Asano, Y. Tanaka, and S. Noda, "On-demand transfer of trapped photons on a chip," Sci. Adv. **2**, e1501690 (2016).
[18]R. Konoike, T. Asano, and S. Noda, "On-chip dynamic time reversal of light in a coupled-cavity system," APL Photonics **4**, 030806 (2019).
[19]K. Srinivasan and O. Painter, "Momentum space design of high-Q photonic crystal optical cavities," Opt. Express **10**, 670–684 (2002).
[20]D. Englund, I. Fushman, and J. Vučković, "General recipe for designing photonic crystal cavities," Opt. Express **13**, 5961–5975 (2005).
[21]Y. Tanaka, T. Asano, and S. Noda, "Design of photonic crystal nanocavity with Q-factor of ~109," J. Light. Technol. **26**, 1532–1539 (2008).
[22]T. Tanabe, M. Notomi, E. Kuramochi, A. Shinya, and H. Taniyama, "Trapping and delaying photons for one nanosecond in an ultrasmall high-Q photonic-crystal nanocavity," Nat. Photonics **1**, 49–52 (2007).
[23]F. Alpeggiani, L. C. Andreani, and D. Gerace, "Effective bichromatic potential for ultra-high Q-factor photonic crystal slab cavities," Appl. Phys. Lett. **107**, 261110 (2015).
[24]A. Simbula, M. Schatzl, L. Zagaglia, F. Alpeggiani, L. C. Andreani, F. Schäffler, T. Fromherz, M. Galli, and D. Gerace, "Realization of high-Q/V photonic crystal cavities defined by an effective Aubry–André–Harper bichromatic potential," APL Photonics **2**, 056102 (2017).
[25]T. Yamamoto, M. Notomi, H. Taniyama, E. Kuramochi, Y. Yoshikawa, Y. Torii, and T. Kuga, "Design of a high-Q air-slot cavity based on a width-modulated line-defect in a photonic crystal slab," Opt. Express **16**, 13809–13817 (2008).
[26]T. Asano, B.-S. Song, and S. Noda, "Analysis of the experimental Q factors (~1 million) of photonic crystal nanocavities," Opt. Express **14**, 1996–2002 (2006).
[27]M. Minkov and V. Savona, "Automated optimization of photonic crystal slab cavities," Sci. Rep. **4**, 05124 (2014).
[28]Y. Lai, S. Pirotta, G. Urbinati, D. Gerace, M. Minkov, V. Savona, A. Badolato, and M. Galli, "Genetically designed L3 photonic crystal nanocavities with measured quality factor exceeding one million," Appl. Phys. Lett. **104**, 241101 (2014).
[29]T. Nakamura, Y. Takahashi, Y. Tanaka, T. Asano, and S. Noda, "Improvement in the quality factors for photonic crystal nanocavities via visualization of the leaky components," Opt. Express **24**, 9541–9549 (2016).
[30]K. Maeno, Y. Takahashi, T. Nakamura, T. Asano, and S. Noda, "Analysis of high-Q photonic crystal L3 nanocavities designed by visualization of the leaky components," Opt. Express **25**, 367–376 (2017).
[31]U. P. Dharanipathy, M. Minkov, M. Tonin, V. Savona, and R. Houdré, "High-Q silicon photonic crystal cavity for enhanced optical nonlinearities," Appl. Phys. Lett. **105**, 101101 (2014).
[32]M. Minkov, V. Savona, and D. Gerace, "Photonic crystal slab cavity simultaneously optimized for ultra-high Q/V and vertical radiation coupling," Appl. Phys. Lett. **111**, 131104 (2017).
[33]E. Kuramochi, M. Notomi, S. Mitsugi, A. Shinya, T. Tanabe, and T. Watanabe, "Ultrahigh-Q photonic crystal nanocavities realized by the local width modulation of a line defect," Appl. Phys. Lett. **88**, 041112 (2006).
[34]In this report, we use Q values excluding the load of the excitation waveguide (unloaded Q) when we compare results of different reports, except for the Q_{exp} values of the heterostructure cavities for which only Q values including the load of the excitation waveguide (loaded Q) have been reported.
[35]T. Asano and S. Noda, "Optimization of photonic crystal nanocavities based on deep learning," Opt. Express **26**, 32704–32716 (2018).
[36]M. Nakadai, K. Tanaka, T. Asano, Y. Takahashi, and S. Noda, "Statistical evaluation of Q factors of fabricated photonic crystal nanocavities designed by using a deep neural network," Appl. Phys. Express **13**, 012002 (2019).
[37]R. Abe, T. Takeda, R. Shiratori, S. Shirakawa, S. Saito, and T. Baba, "Optimization of an H0 photonic crystal nanocavity using machine learning," Opt. Lett. **45**, 319–322 (2020).
[38]Z. Lin, M. Lončar, and A. W. Rodriguez, "Topology optimization of multi-track ring resonators and 2D microcavities for nonlinear frequency conversion," Opt. Lett. **42**, 2818–2821 (2017).
[39]T. Asano and S. Noda, "Iterative optimization of photonic crystal nanocavity designs by using deep neural networks," Nanophotonics **8**, 2243–2256 (2019).
[40]T. Asano and S. Noda, "Optimization of a photonic cavity based on repeated search using machine learning," in The 80th JSAP Autumn Meeting, 20a-B01-7, Hokkaido, Japan, September 2019.
[41]J. P. Vasco and V. Savona, "Global optimization of an encapsulated Si/SiO_2 L3 cavity for ultra-high quality factor," arXiv:1911.03361v2.
[42]H. Hagino, Y. Takahashi, Y. Tanaka, T. Asano, and S. Noda, "Effects of fluctuation in air hole radii and positions on optical characteristics in photonic crystal heterostructure nanocavities," Phys. Rev. B **79**, 085112 (2009).
[43]Y. Taguchi, Y. Takahashi, Y. Sato, T. Asano, and S. Noda, "Statistical studies of photonic heterostructure nanocavities with an average Q factor of three million," Opt. Express **19**, 11916–11921 (2011).
[44]H. Sekoguchi, Y. Takahashi, T. Asano, and S. Noda, "Photonic crystal nanocavity with a Q-factor of ~9 million," Opt. Express **22**, 916–924 (2014).
[45]M. Borselli, T. J. Johnson, and O. Painter, "Measuring the role of surface chemistry in silicon microphotonics," Appl. Phys. Lett. **88**, 131114 (2006).
[46]A. Chutinan, M. Mochizuki, M. Imada, and S. Noda, "Surface-emitting channel drop filters using single defects in two-dimensional photonic crystal slabs," Appl. Phys. Lett. **79**, 2690–2692 (2001).
[47]Y. Takahashi, H. Hagino, Y. Tanaka, B.-S. Song, T. Asano, and S. Noda, "High-Q nanocavity with a 2-ns photon lifetime," Opt. Express **15**, 17206–17213 (2007).
[48]D. G. Hall, "In-plane scattering in planar optical waveguides: Refractive-index fluctuations and surface roughness," J. Opt. Soc. Am. A **2**, 747–752 (1985).
[49]M. Minkov, U. P. Dharanipathy, R. Houdré, and V. Savona, "Statistics of the disorder-induced losses of high-Q photonic crystal cavities," Opt. Express **21**, 28233–28245 (2013).